IChemE

0263–8762/01/$10.00+0.00

Trans IChemE, Vol. 79, Part A, March 2001

EXPLOITING CONFIGURATIONAL ENTROPY EFFECTS FOR SEPARATION OF HEXANE ISOMERS USING SILICALITE-1

R. KRISHNA

Department of Chemical Engineering, University of Amsterdam, Amsterdam, The Netherlands

The sorption isotherms for binary mixtures of (a) *n*-hexane (*n*-C_6) and 3-methylpentane (3MP), and (b) *n*-C_6 and 2,2 dimethylbutane (22DMB) in silicalite-1 have been determined using Configurational Bias Monte-Carlo (CBMC) simulation techniques. Due to differences in the packing efficiencies of the linear and branched alkanes, the sorption selectivity is in favour of the linear alkane. At high loadings, configurational entropy effects are seen to virtually exclude the branched alkane from the silicalite matrix. Using the Maxwell-Stefan diffusion theory, it is shown that this configurational entropy effect results in curious membrane permeation, uptake and breakthrough characteristics. Configurational entropy effects can be exploited to achieve high separation selectivities for hexane isomers.

Keywords: Configurational-Bias Monte Carlo simulations; Maxwell-Stefan theory; Dual-site Langmuir isotherm; Real Adsorbed Solution Theory; transient uptake; adsorber breakthrough.

1. INTRODUCTION

The separation of isomers of alkanes is a problem that is growing in industrial importance. New reformulated gasoline specifications are forcing petroleum refiners to reduce the amount of olefins and aromatics in gasoline and consequently, there is a greater need for catalytic isomerization for converting straight chain hydrocarbons to branched hydrocarbons in the refining industry. Branched hydrocarbons are preferred to straight-chain hydrocarbons as ingredients in petrol because branched hydrocarbons burn more efficiently and have a higher octane number. Consider, for example, the isomers of hexane; *n*-hexane has a RON (Research Octane Number) = 30 whereas the double branched isomer, 2,3 dimethylbutane (23DMB) has a RON = 105; see Figure 1. In the catalytic isomerization process, straight-chain hydrocarbons are converted to their mono- or di-branched structures. However, the product of catalytic isomerization is a mixture of linear and branched hydrocarbons that are in thermodynamic equilibrium and the separation of linear hydrocarbons from their branched isomers becomes necessary; a typical process flowsheet is shown in Figure 2. The separation of the hydrocarbon isomers is usually carried out using adsorption in a bed of zeolite 5A particles[1,2]. The principle of separation is molecular sieving; see Figure 3. Only the linear paraffin is capable of entering the pores of 5A zeolite and the branched isomers are excluded. One important disadvantage of sorption separation using 5A zeolite is that the diffusivities, and hence the fluxes, are very low. Therefore equipment sizes are large.

The purpose of this paper is to discuss and develop a new separation principle for sorption separation of hydrocarbon isomers which utilises subtle configurational entropy effects using silicalite as sorbent. It considers the specific example of the separation of the isomers of hexane; this mixture is of particular importance because they are important constituents of gasoline.

In Section 2 the separation principle of utilising configurational entropy effects is explained in qualitative terms. In Section 3 determines, the required sorption isotherms for mixtures of hexane isomers, using Configurational-Bias Monte Carlo (CBMC) techniques. The configurational entropy-driven separation concept could be realised in practice using two alternative configurations:

(a) steady-state permeation across a silicalite-1 membrane; and
(b) adsorption in a packed bed of silicalite particles.

In order to calculate the permeation rates and breakthrough curves we need to describe mass transfer within silicalite. For this purpose we use the Maxwell-Stefan theory for diffusion, a refresher to this theory is presented in Section 4. Section 5 presents simulations for a membrane permeation device. Section 6 determines breakthrough curves in a packed adsorber.

2. ORDERING OR CONFIGURATIONAL ENTROPY EFFECTS

A careful examination of the physical properties of linear and branched alkanes[3], shows that the largest difference between these isomers is with respect to the freezing point; see data shown in Figure 4. When a mixture of say *n*-C_6 and 2MP is cooled, the first crystals to form will be that of the linear isomer because the linear paraffin molecules ''stack'' more easily. Branching destroys the symmetry

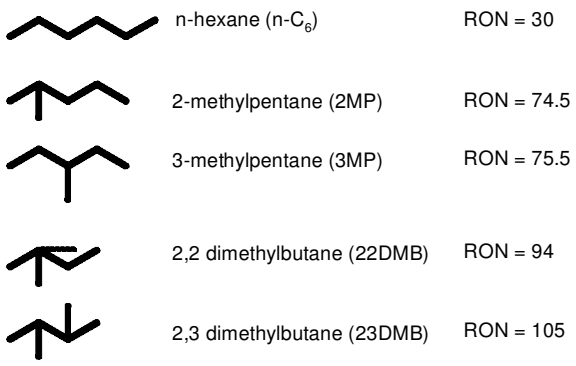

Figure 1. Research Octane Numbers (RON) of hexane isomers.

required for crystal formation. In other words, the differences in the freezing points are due to differences in ''ordering'' or ''packing efficiencies''. The major drawback in applying this principle to separate linear and branched alkanes is the very low temperatures to which the mixtures must be cooled, of the order of 120–180 K. Therefore freeze crystallisation is not a viable technological solution for separation of isomers in the 4–9 C atom range, of interest as components in gasoline.

Ideally exploitation of packing efficiency, or configurational entropy, differences should be possible, without the need to cool to the low temperatures required for crystallisation. To achieve this goal adsorption of the hexane isomers inside the matrix of an ordered structure, such as silicalite-1 is considered; see Figure 5. Silicalite consists of straight channels and zig-zag channels, which cross each other at intersections. The length of the normal hexane molecule is commensurate with the length of the zig-zag channel, between two intersections[4]. These linear hexane molecules pack more efficiently within the silicalite structure; this is also evidenced by the differences in the saturation loadings, expressed in molecules per unit cell, between linear and branched alkanes in silicalite; see Figure 6. The maximum loadings for hexane isomers are as follows; *n*-C_6: 8, 2MP: 6.2; 22DMB: 4 molecules per unit cell. This means that for adsorption of pure components at equilibrium, the maximum loadings of 22DMB would be half that of *n*-C_6.

In practice we would need to consider the differences in sorption loadings from bulk fluid mixtures. This raises the problem of determining the sorption isotherms of mixtures.

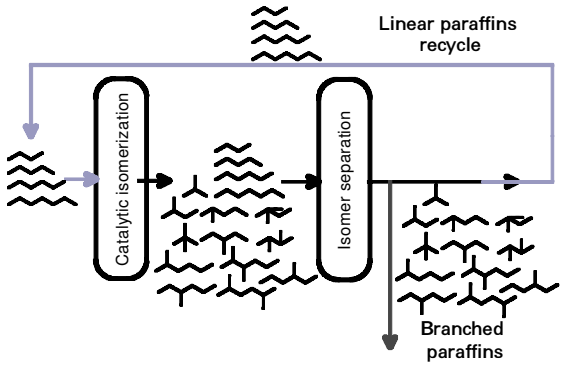

Figure 2. Schematic of catalytic isomerisation process.

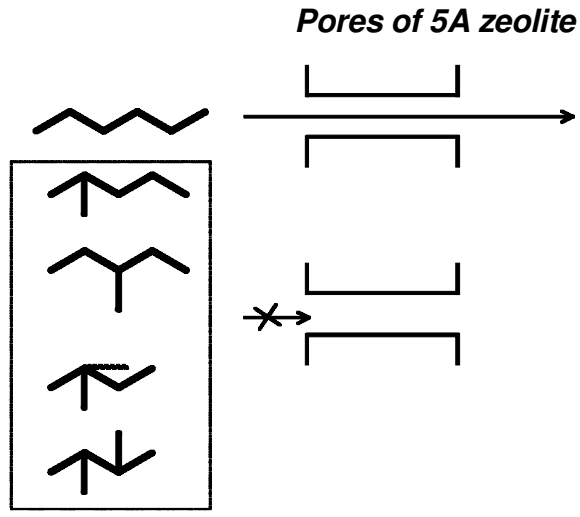

Figure 3. Schematic showing the sieving principle of zeolite 5A for separating *n*-hexane from its isomers.

3. CBMC SIMULATIONS OF PURE COMPONENT AND MIXTURE ISOTHERMS

While there is a considerable amount of published experimental data on pure component isotherms for various hydrocarbons[5,6] on silicalite, there is very little data on mixture isotherms. This lack of data is most probably due to the difficulty of experimentation. Earlier publications[7–13] have shown the power of CBMC simulations for calculating pure component and mixture isotherms for normal and branched alkanes in silicalite. For linear and branched alkanes in silicalite, Vlugt *et al.*[11] have provided a detailed comparison of pure component isotherms estimated from CBMC techniques with published experimental data to demonstrate the accuracy of CBMC simulations; this work was of a fundamental nature, and not geared towards process development. In the current work, further

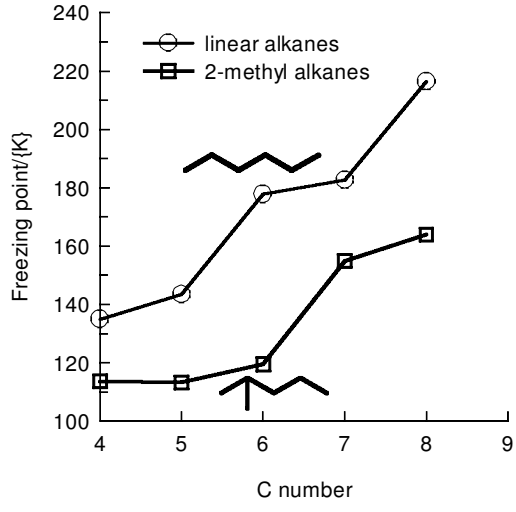

Figure 4. Freezing point of linear and 2-methyl alkanes.

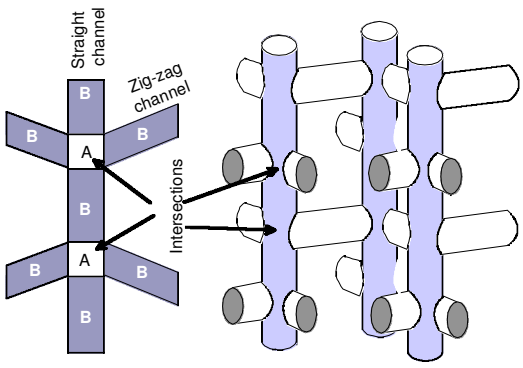

Figure 5. Schematic of silicalite structure indicating the sorption sites indicating the channel intersections (A) and channel interiors (B), consisting of straight and zig-zag channels.

pure component and 50-50 mixture isotherms in silicalite-1 have been carried out for the following systems:

a) *n*-hexane (*n*-C_6)—3-methyl pentane (3MP) at 362 K; and
b) *n*-hexane (*n*-C_6)—2,2 dimethyl butane (22DMB) at 398 K.

At the chosen temperatures the hydrocarbon mixtures are in the vapour phase. Later in this paper two technological separation devices are examined:

(i) a silicalite membrane permeation module; and
(ii) a packed bed adsorber.

A further reason for choosing these temperatures is that experimental data on membrane permeation is available for these two mixture under the simulated conditions[14,15].

Simulations have been performed in the Grand Canonical ensemble where the zeolite is in contact with a reservoir that fixes the chemical potential of each component and the temperature. In a CBMC simulation, it is essential to exchange particles successfully with the reservoir. With this technique a flexible alkane molecule is grown atom by atom so that the 'empty spaces' in the zeolite are found. The bias of this growing scheme is removed exactly by a modification of the acceptance rules[11,16]. The acceptance ratio of the particle exchange move is increased by 10 to 100 orders of magnitude and thus makes these simulations possible. To increase the efficiency for the mixture simulations, we also performed trial moves which change the identity of a particle. The linear and branched alkanes are described with a united-atom model, i.e. CH_3, CH_2 and CH groups are considered as single interaction centers. The zeolite is assumed to be rigid and the interactions of the alkane with the zeolite are dominated by the oxygen atoms of the zeolite. The alkane-zeolite and alkane-alkane interactions are described by a Lennard-Jones potential. The intra-molecular interactions include bond-bending and torsion potentials and a fixed C-C bond-length. The force-field parameters are reported in Vlugt *et al.*[11].

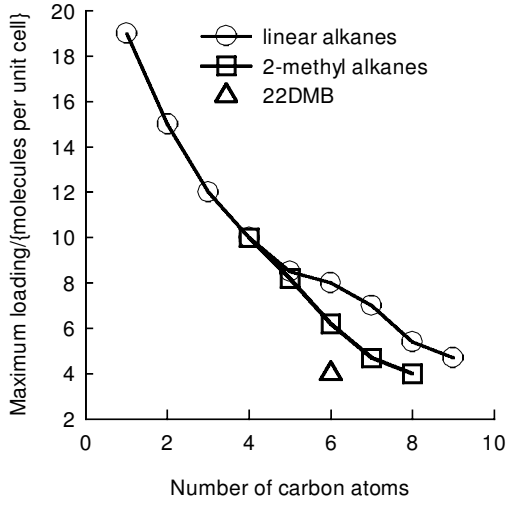

Figure 6. Saturation loadings (molecules per unit cell) of alkanes in silicalite-1 obtained from CBMC simulations.

The simulation box consists of 16 ($2 \times 2 \times 4$) unit cells of silicalite. Simulations are performed in cycles, in each cycle an attempt is made to perform one of the following moves:

(1) displacement of a chain, a chain is selected at random and given a random displacement;
(2) rotation of a chain, a chain is selected at random and given a random rotation around the center of mass;
(3) partial regrowing of a chain, a chain is selected at random and part of the molecule is regrown using the CBMC scheme;
(4) exchange with reservoir using the CBMC scheme, it is decided at random whether to add or to remove a molecule from the zeolite; and
(5) change of identity (only in the case of mixtures), one of the components is selected at random and an attempt is made to change its identity.

The acceptance rules for this type of move are given elsewhere[11]. A total simulation consisted of at least 300,000 Monte Carlo cycles.

Modelling the Pure Component Isotherms

For the pure components, the Dual-site Langmuir (DSL) model was found to be applicable for the components studied. The DSL model for the loading, expressed in molecules per unit cell, is:

$$\Theta_i^0(P) = \frac{\Theta_{i,sat,A} b_{i,A} P}{1 + b_{i,A} P} + \frac{\Theta_{i,sat,B} b_{i,B} P}{1 + b_{i,B} P} \qquad (1)$$

which gives a good description of the pure component isotherms; see e.g. Figure 7 (a). Vlugt *et al.*[11] have shown that the DSL model provides an excellent representation of the isotherms for both linear and branched alkanes for a wide range of carbon numbers. The superscript 0 on $\Theta_i^0(P)$ is used to emphasise that the relation is for pure component loadings. For silicalite-1 a molecular loading of 4 molecules per unit cell corresponds to 0.6935 mol kg^{-1} and therefore the molar loading, $q_i^0(P)$, is given by the following expression:

$$\frac{q_i^0(P)}{\text{mol kg}^{-1}} = \frac{\Theta_i^0(P)}{[\text{molecules per unit cell}]} \times \frac{0.6935}{4} \qquad (2)$$

In equation (1) the subscripts A and B refer to two sorption sites within the silicalite structure, with different sorption capacities and sorption strengths:

(1) Site A, which represents the intersections between the straight channels and the zig-zag channels; and

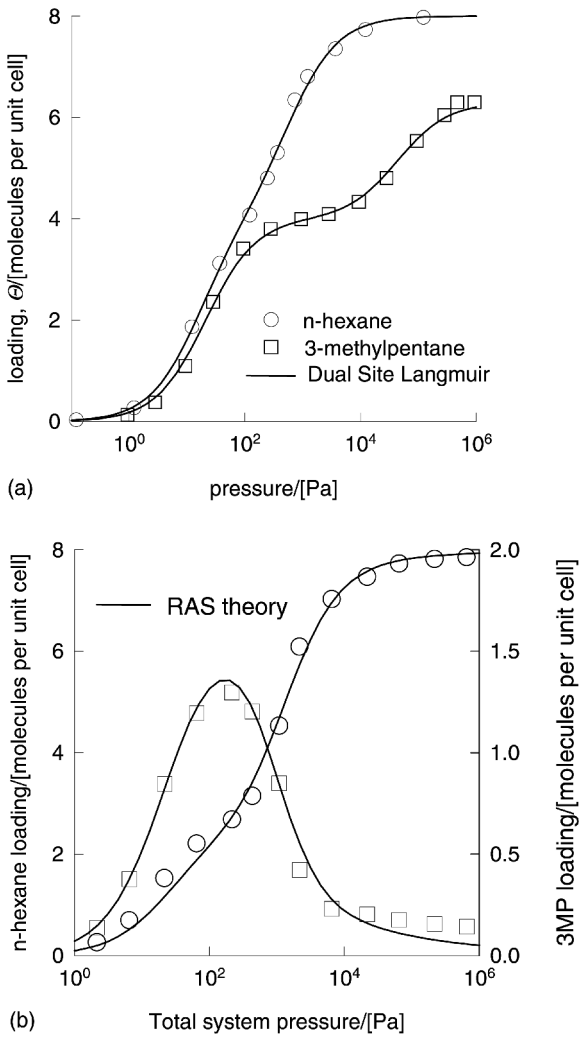

Figure 7. (a) Pure component and (b) mixture loadings for *n*-hexane (1)—3MP2(2) at 362 K in silicalite.

(2) Site B, which represents the channel interiors; see Figure 5.

Note from Figure 7(a) that the isotherm for 3MP exhibits an inflection at a loading of 4 molecules per unit cell. The inflection in the isotherm is due to the preferential location of 3MP at the intersections. However, at a loading, Θ, of 4 molecules per unit cell (corresponding to 0.6935 mol/kg of silicalite) all the intersections are fully occupied. To obtain loadings higher than 4, these molecules must seek residence in the channel interiors, which is energetically more demanding. This leads to an inflection in the isotherm.

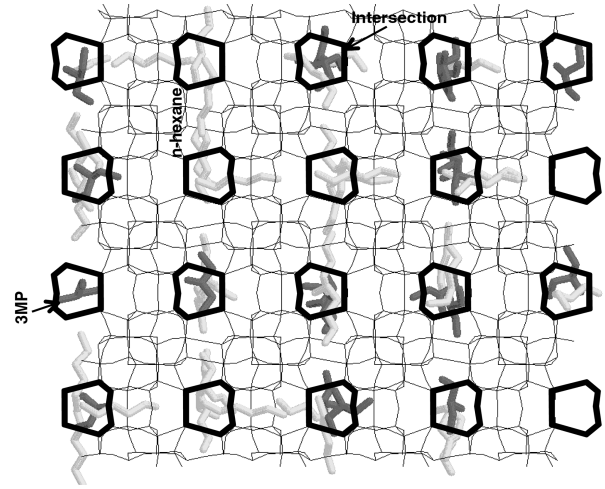

Figure 8. Snapshot showing the location of a 50-50 mixture of *n*-hexane (1)–3MP (2) at 362 K and 100 Pa. Preferential siting of 3 MP at the intersections between the straight and zig-zag channels is evident. The linear alkane can be located at any position within the silicalite structure.

The fitted parameters for the pure component isotherms are listed in Table 1. Both differences in the saturation capacities and molecular configurations are important determinants of the sorption selectivity, S, defined by:

$$S = \frac{\Theta_1/\Theta_2}{p_1/p_2} \tag{3}$$

In equation (3) the Θ_i refer to loadings of the components in the mixture within the zeolite.

CBMC Mixture Simulations

The 50-50 mixture isotherms for *n*-hexane and 3-methyl pentane calculated from CBMC simulations are shown in Figure 7(b). The branched alkane 3MP exhibits a curious maximum with respect to molecular loading within the silicalite structure. As the partial pressures increase to 100 Pa, the sorbate loading of both linear and branched alkanes increase till a maximum is reached in the loading of 3MP. This occurs at a total loading of 4 molecules per unit cell. Up to this point there is really no competition between n-C_6 and 3MP and both are almost equally easily adsorbed. Examination of a snapshot of the molecular sitings at 100 Pa shows that all the 3MP molecules are located at the intersections between the straight channels

Table 1. Pure component parameters for dual-site Langmuir model.

		Dual-Site Langmuir Parameters, see equation (1)			
		Site A		Site B	
Component i	Temperature, K	$b_{i,A}$, Pa^{-1}	$\Theta_{i,sat,A}$, molecules per unit cell	$b_{i,B}$ Pa^{-1}	$\Theta_{i,sat,B}$ molecules per unit cell
n-hexane	362	6.32×10^{-2}	4.0	1.7×10^{-3}	4.0
	398	8.1×10^{-3}	4.0	1.6×10^{-4}	4.0
3-methyl pentane	362	4.75×10^{-2}	4.0	2.27×10^{-5}	2.3
2,2 dimethyl butane	398	1.6×10^{-3}	4.0		0

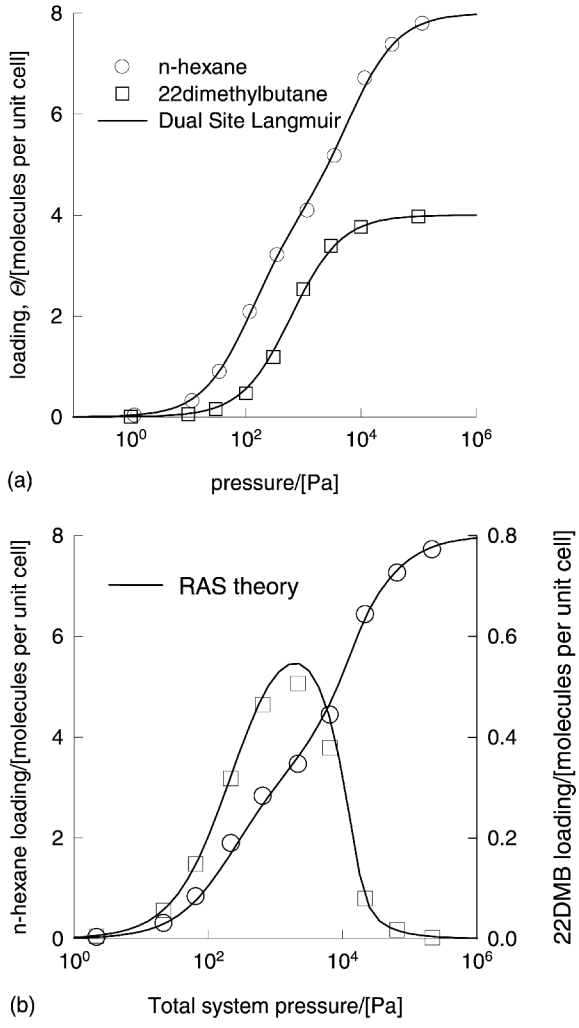

Figure 9. (a) Pure component and (b) mixture loadings for *n*-hexane (1)—22DMB (2) at 398 K in silicalite.

and the zigzag channels whereas *n*-C_6 are located everywhere; see Figure 8. The *n*-C_6 molecules fit nicely into both straight and zigzag channels[4]; these molecules have a higher ''packing efficiency'' than 3MP. As the pressure is increased beyond 100 Pa, it is more efficient to obtain higher loading by ''replacing'' the 3MP with *n*-C_6; this configurational entropy effect is the reason behind the curious maximum in the 3MP isotherm.

For the mixture *n*-hexane–22DMB, a similar result is obtained; see Figure 9. Again note the curious maximum in the 22DMB loading when the mixture loading corresponds to 4 molecules per unit cell. The snapshot in Figure 10 reveals that the 22DMB molecule prefers to reside at the intersections whereas the *n*-C_6 molecule is located everywhere.

From the mixture isotherms shown in Figures 7 and 9, it is clear that high selectivities for separation of linear and branched alkanes can be obtained provided conditions inside the zeolite are maintained so as to correspond to the conditions on the right side of the ''mountain'' or peak of the loading of the branched isomer in the 50-50 mixture.

To carry out process design calculations mixture behaviour also needs to be modelled.

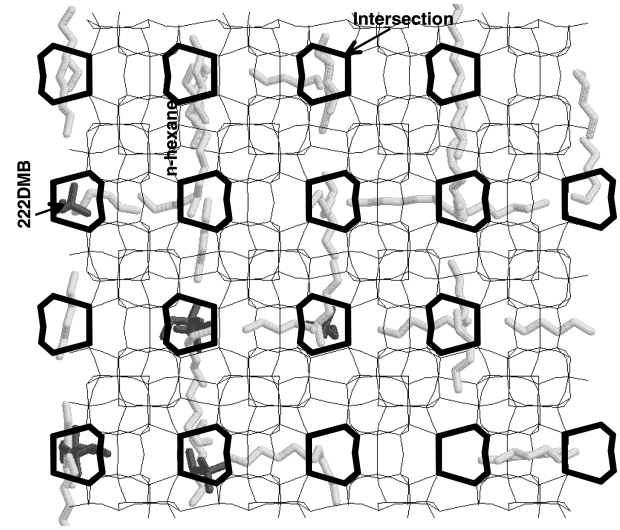

Figure 10. Snapshot showing the location of a 50-50 mixture of *n*-hexane (1)–22DMP (2) at 373 K and 500 Pa. Preferential siting of 22DMB at the intersections between the straight and zig-zag channels is evident.

Modelling the Mixture Isotherms using the RAS Theory

In order to model the mixture isotherms seen in Figure 7(b) and 9(b), the Real Adsorbed Solution (RAS) theory is used. The basis of this theory is the relation:

$$Py_i = P_i^0(\pi)x_i\gamma_i \tag{4}$$

which is the analog of the equation commonly used to describe vapour-liquid equilibrium. In equation (4) x_i is the mole fraction in the adsorbed phase, defined as:

$$x_i = \frac{\Theta_i}{\Theta_1 + \Theta_2} \tag{5}$$

and $P_i^0(\pi)$ is the pressure which for sorption of every pure component i, yields the same spreading pressure, π, as that for the mixture. The spreading pressure is defined by the Gibbs adsorption isotherm:

$$\frac{\pi A}{RT} = \int_{P=0}^{P=P_i^0} \frac{q_i^0(P)}{P}dP \tag{6}$$

where A is the surface area of the adsorbent and $\Theta_i^0(P)$ is the pure component isotherm given by equation (1). Absolute rather than excess adsorption properties are described by equation (6). The total amount adsorbed is obtained from:

$$\Theta_1 + \Theta_2 = \frac{1}{\dfrac{x_1}{\Theta_1^0(P_1^0)} + \dfrac{x_2}{\Theta_2^0(P_2^0)}} \tag{7}$$

Following the work of Calleja *et al.*[17] we have used the Wilson model for the activity coefficients:

$$\begin{aligned}\ln(\gamma_1) &= 1 - \ln(x_1 + x_2\Lambda_{12}) - \frac{x_1}{x_1 + x_2\Lambda_{12}} \\ &\quad - \frac{x_2\Lambda_{21}}{x_2 + x_1\Lambda_{21}} \\ \ln(\gamma_2) &= 1 - \ln(x_2 + x_1\Lambda_{21}) - \frac{x_2}{x_2 + x_1\Lambda_{21}} \\ &\quad - \frac{x_1\Lambda_{12}}{x_1 + x_2\Lambda_{12}}\end{aligned} \tag{8}$$

Table 2. Wilson non-ideality parameters for mixture isotherms.

Mixture	Temperature, K	Wilson parameters Λ_{12}	Λ_{12}
(a) *n*-hexane–3-methyl pentane	362	1.01	0.215
(b) *n*-hexane–2,2 dimethyl butane	398	2.6	0.01

Using the CBMC mixture simulations, the values of the fitted Wilson parameters can be fitted; these values given in Table 2. For both mixtures the activity coefficients deviate significantly from unity, indicating strong non-ideality. From Figures 7(b) and 9(b) we see that the RAST provides a good description of the mixture behaviour.

4. THE MAXWELL-STEFAN THEORY FOR MIXTURE DIFFUSION

For calculating the membrane permeation rates and adsorber breakthrough curves diffusion on the hexane isomers, at high loadings, within silicalite requires description. In developing the equations for diffusion of two components within a zeolite, the zeolite itself is treated as a pseudo species and the fractional occupancies are considered to be analogous to mole fractions. Following the treatment of Krishna and others[18–25]:

$$-\rho\frac{\theta_i}{RT}\nabla\mu_i = \sum_{\substack{j=1\\ j\neq i}}^{2}\frac{\Theta_j\mathbf{N}_i - \Theta_i\mathbf{N}_j}{\Theta_{i,sat}\Theta_{j,sat}Đ_{ij}} + \frac{\mathbf{N}_i}{\Theta_{i,sat}Đ_i}; \quad i = 1,2 \tag{9}$$

where the fractional occupancy θ_i of the sorbate within the zeolite matrix is defined as:

$$\theta_i \equiv \Theta_i/\Theta_{i,sat}: \qquad i = 1,2 \tag{10}$$

where $\Theta_{i,sat}$ are the saturation loadings of species i in the zeolite. In general the saturation loadings of the linear and branched alkanes are different; see Table 1.

In the Maxwell-Stefan formulation for zeolite diffusion, equation (9), two types of Maxwell-Stefan diffusivities must be considered in general: $Đ_{ij}$ and $Đ_i$. The $Đ_i$ are the same diffusivites as encountered in single component diffusion. Mixture diffusion introduces an additional complication due to sorbate-sorbate interactions. This interaction is embodied in the coefficients $Đ_{ij}$. This coefficient can be considered as representing the facility for counter-exchange, i.e. at a sorption site the sorbed species j is replaced by the species i. The net effect of this counter-exchange is a slowing down of a faster moving species due to interactions with a species of lower mobility. Also, a species of lower mobility is accelerated by interactions with another species of higher mobility. With the aid of kinetic Monte Carlo simulations, Paschek and Krishna[25] have shown that the interchange coefficient is a measure of correlation effects during molecular jumps. The two types of Maxwell-Stefan diffusivities are portrayed in Figure 11. In the inset to Figure 10 $Đ_{12}$ is portrayed as representing the ease with which species 1 is replaced by species 2.

A procedure for the estimation of the counter-sorption diffusivity has been suggested by Krishna[18] based on the generalisation of Vignes[26] relationship for diffusion in bulk liquid mixtures:

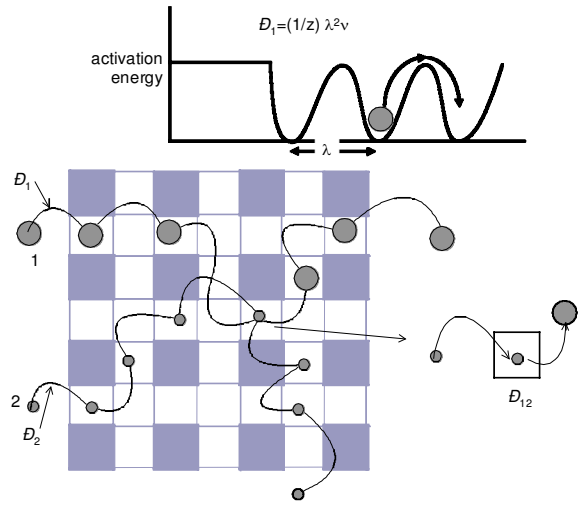

Figure 11. Pictorial representation of the Maxwell-Stefan diffusivities.

$$Đ_{12} = [Đ_1]^{\theta_1/(\theta_1+\theta_2)}[Đ_2]^{\theta_2/(\theta_1+\theta_2)} \tag{11}$$

which is essentially a logarithmic interpolation formula between the values of $Đ_i$ and $Đ_j$. The validity of the Maxwell-Stefan formulation, given by equations (10) and (11), has been established by comparison with experiments[13,21] and Molecular Dynamics simulations[23,24].

The chemical potential gradients in equation (9) may be expressed in terms of the gradients of the occupancies by introduction of the matrix of thermodynamic factors $[\Gamma]$

$$\frac{\theta_i}{RT}\nabla\mu_i = \sum_{j=1}^{n}\Gamma_{ij}\nabla\theta_j; \quad \Gamma_{ij} \equiv \left(\frac{\Theta_{j,sat}}{\Theta_{i,sat}}\right)\frac{\Theta_i}{p_i}\frac{\partial p_i}{\partial P_j};$$

$$i,j = 1,2 \tag{12}$$

The elements of $[\Gamma]$ have to be determined by (numerical) differentiation of the RAST isotherm model described by equations (4)–(8).

Combining equations (9) and (12) an explicit expression can be written for the fluxes $\mathbf{N}_i$ using n-dimensional matrix notation:

$$(\mathbf{N}) = -\rho[\Theta_{sat}\mathbf{I}B]^{-1}[\Gamma]\nabla(\theta) \tag{13}$$

where the elements of the matrix $[B]$ are:

$$B_{ii} = \frac{1}{Đ_i} + \sum_{\substack{j=1\\ j\neq 1}}^{n}\frac{\theta_j}{Đ_{ij}}; \qquad B_{ij} = -\frac{\theta_i}{Đ_{ij}};$$

$$i,j = 1,2 \tag{14}$$

and $[\Theta_{sat}]$ is a diagonal matrix of saturation capacities:

$$[\Theta_{sat}] = \begin{bmatrix}\Theta_{i,sat} & 0\\ 0 & \Theta_{2,sat}\end{bmatrix} \tag{15}$$

The more commonly used Fick diffusivity matrix is defined as:

$$(\mathbf{N}) = -\rho[\Theta_{sat}\mathbf{I}D]\nabla(\theta) \tag{16}$$

Comparing equations (13) and (16) we obtain the following inter-relation between the Fick and the Maxwell-Stefan diffusivities:

$$[D] = [B]^{-1}[\Gamma]; \qquad [B]^{-1} = [D\mathbf{I}\Gamma]^{-1} \tag{17}$$

The thermodynamic correction factor matrix $[\Gamma]$ is

generally non-diagonal and has a significant influence on the diffusion behaviour of mixtures.

For a binary mixture, we could force-fit equation (13) for the two fluxes $\mathbf{N}_i$ into the form of Fick's law for each species:

$$\mathbf{N}_i = -\rho\Theta_{i,sat} D_{i,eff} \nabla\theta_i; \qquad i = 1,2 \tag{18}$$

where the effective Fick diffusivities of components 1 and 2 are given by:

$$D_{1,eff} = D_{11} + D_{12}\frac{\nabla\theta_2}{\nabla\theta_1} \tag{19}$$

$$D_{2,eff} = D_{21}\frac{\nabla\theta_1}{\nabla\theta_2} + D_{22} \tag{20}$$

Equations (19) and (20) are generalisations of the Habgood relations commonly used in the zeolite diffusion literature[27,28].

The equation (13) is used for calculation of the fluxes of species 1 (linear n-C_6) and 2 (branched 3MP or 22DMB) for two cases:

(1) permeation across a membrane; and
(2) breakthrough in a packed bed adsorber.

5. PERMEATION OF HEXANE ISOMERS ACROSS SILICALITE MEMBRANE

First, consider binary mixture permeation across a silicalite membrane. The membrane, of thickness δ, separates two well mixed compartments; see Figure 12. Ignoring the mass transfer resistances external to the membrane and considering the transfer fluxes to be determined solely by intra-(microporous)-membrane transport. At time $t = 0$, a gaseous mixture is introduced into the left compartment at pressure p_0 and this composition is maintained throughout the experiment. The downstream compartment is maintained at a pressure p_δ. Interest is in the determination of the transient fluxes till steady state is reached.

The interior of the membrane is initially considered to be totally uncovered by the transferring species, i.e.:

$$t = 0, \qquad 0 \le z \le \delta; \qquad \theta_{iz} = 0 \tag{21}$$

At the left fluid-membrane interface the equilibrium relation using the RAST isotherm is described by equations (4)–(8).

The right membrane compartment is assumed to be swept with an inert gas, maintaining the partial pressures of both the permeating species close to zero. Therefore the following condition is used at the right fluid-membrane interface:

$$t \ge 0, \quad z = \delta; \qquad \theta_{i\delta} = 0 \tag{22}$$

The differential equations describing the transient surface occupancies are:

$$\frac{\partial\theta_i}{\partial t} = -\frac{1}{\rho\Theta_{i,sat}}\frac{\partial N_i}{\partial z}; \quad N_i = -\rho\Theta_{i,sat} D_{i,eff}\frac{\partial\theta_i}{\partial z}; \quad i = 1,2 \tag{23}$$

The set of two coupled partial differential equations (23) subject to the initial and boundary conditions (21) and (22) were solved using the method of lines[29] to determine the fluxes; the details regarding the numerical procedures used has been described in earlier work[30].

Transient simulations for a 50-50 mixture of n-C_6 and 3MP at 362 K across a silicalite membrane shown schematically in Figure 13(a) for a specific situation in which the upstream total hydrocarbons pressure is 2000 Pa. Figure 13(a) shows a plot of the dimensionless flux, $N_i\delta/\rho Đ_i\Theta_{i,sat}$ against the dimensionless time, defined as $tĐ_1/\delta^2$. Note the curious maximum in the transient flux of 3MP. In Figure 13(b) the steady-state dimensionless fluxes are calculated for various upstream total hydrocarbon pressures. The most remarkable observation concerns the flux of 3MP, which exhibits a maximum at a total upstream pressure of 500 Pa. This implies that for situations in which the upstream pressure is lower than 500 Pa, the flux of 3MP increases when its partial pressure driving force across the membrane increases; this is 'normal' behaviour. However, for situations in which the upstream pressure is higher than 500 Pa, the flux of 3MP decreases when its partial pressure driving force across the membrane increases; this is contrary to normal expectations. The reason for the maximum in the 3MP flux is to be

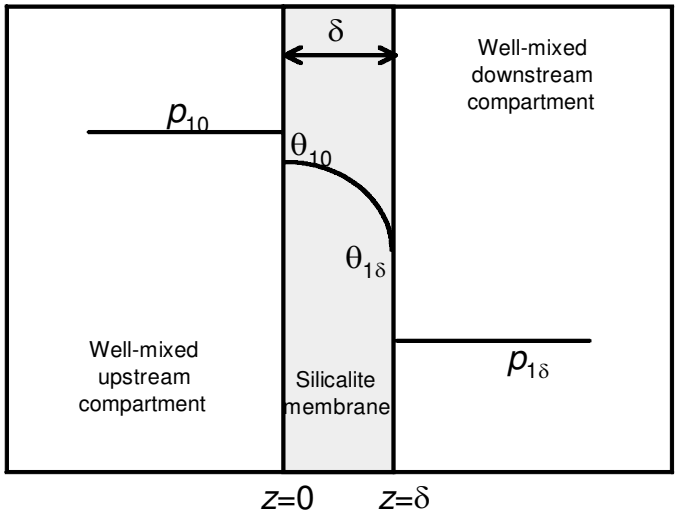

Figure 12. Schematic of silicalite membrane separation process for separation of hydrocarbon mixture.

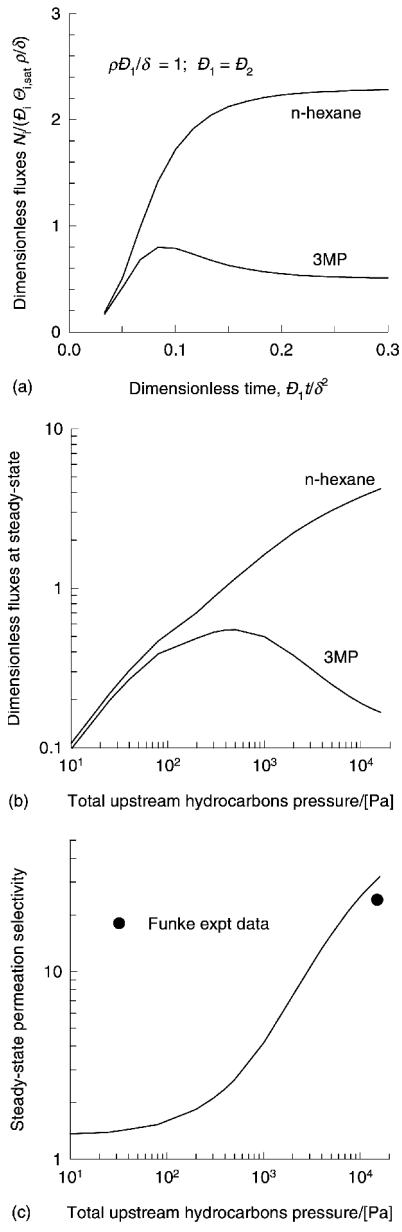

Figure 13. (a) Transient diffusion fluxes for permeation of 50-50 mixture of n-C_6 and 3MP across a silicalite membrane at 362 K. The upstream partial pressures are p_{10} = 1 kPa, p_{20} = 1 kPa. (b) Steady-state permeation fluxes as a function of upstream hydrocarbons pressure. Selectivity: RAST vs IAST, the experimental data point in (c) is from Funke *et al.*[14].

found in the maximum in the loading; see Figure 7(b). The steady-state permeation selectivity, S_P, defined by:

$$S_P = \frac{N_1/N_2}{p_{10}/p_{20}} \tag{24}$$

has been plotted against the upstream hydrocarbons pressure in Figure 13(c). In order to obtain high permeation selectivities the upstream pressure has to be maintained at a level such that the upstream pressures are at least 10 kPa. Also shown in Figure 6(b) is the experimentally observed selectivity of 24 obtained by Funke *et al.*[14]. The experimentally observed selectivity matches very well with our calculations, which did not require any empirical inputs from the experiments of Funke.

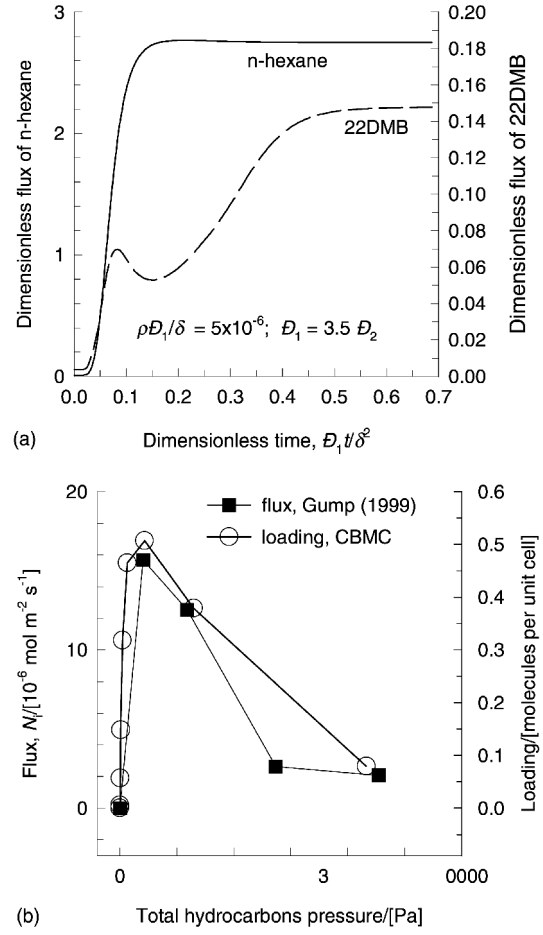

Figure 14. (a) Transient diffusion fluxes for permeation of 50-50 mixture of n-C_6 and 22DMB across a silicalite membrane at 398 K. The upstream partial pressures are p_{10} = 12 kPa, p_{20} = 12 kPa. (b) Measured steady-state permeation flux of 22DMB as a function of upstream hydrocarbons pressure comparred with its loading determined from CBMC simulations. Experimental data of Gump *et al.*[15].

We now consider diffusion of a 50-50 mixture of n-hexane and its isomer 22DMB across a silicalite membrane at a temperature of 398 K for which the mixture isotherm has been shown in Figure 9(b). Figure 14(a) shows the transient fluxes of n-C_6 and 22DMB for an upstream total hydrocarbons pressure of 24 kPa, corresponding to conditions beyond the maximum in its loading in the 50-50 mixture; see Figure 9(b). The curious hump in the 22DMB transient approach to steady-state is to be noted. Figure 14(b) compares the 22DMB flux measured by Gump *et al.*[15] with the 22DMB loading calculated from CBMC simulations. The curious maximum in the flux of 22DMB coincides precisely with the maximum in the 22DMB loading and the Gump experiments can be taken to verify the CBMC mixture simulations. Figure 14(b) should be considered as a direct verification of the configurational entropy effects which determine the selectivity of separation.

6. SELECTIVE SORPTION IN A PACKED BED OF SILICALITE

An alternative to membrane permeation is to separate the isomers by adsorption in a bed packed with silicalite

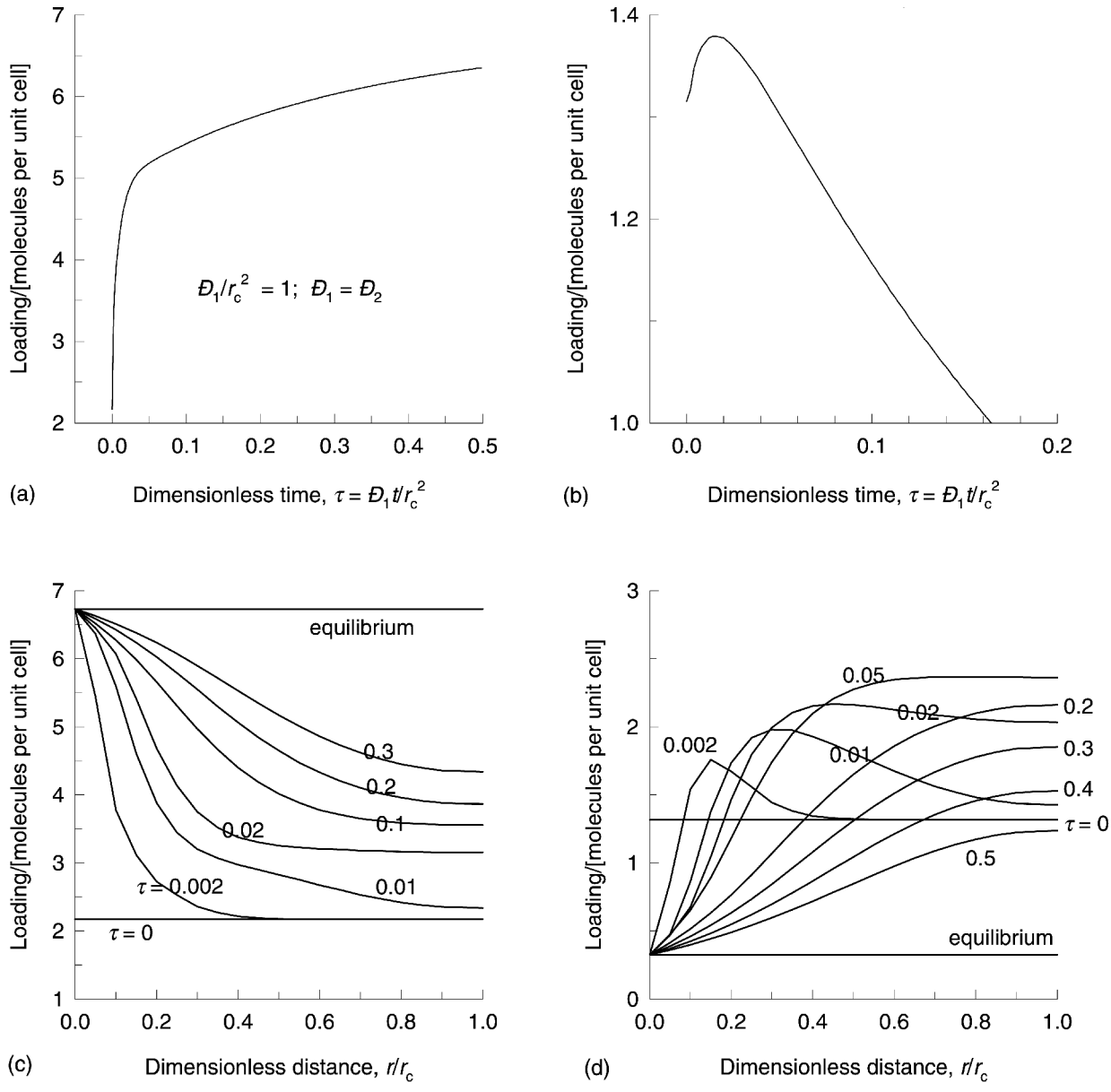

Figure 15. Transient uptake within silicalite particle of (a) *n*-C_6 and (b) 3MP at 362 K. The particle is exposed to a 50-50 mixture at a total hydrocarbons pressure of 5 kPa. The loading profiles within the particle are shown in (c) *n*-C_6 loading within silicalite, and (d) 3MP loading within silicalite.

sorbent particles, of radius r_c. Before considering the performance of the packed bed, examine the transport phenomena within a single spherical particle.

Consider first the transient uptake of *n*-C_6 and 3MP from a 50-50 mixture at 362 K and total pressure of 5 kPa into a spherical crystal of silicalite. The uptake is described by the following set of coupled partial differential equations:

$$\frac{\partial \theta_i}{\partial t} = -\frac{1}{\rho q_{i,sat}} \frac{1}{r^2} \frac{\partial}{\partial r}(r^2 N_i); \qquad N_i = -\rho q_{i,sat} D_{i,eff} \frac{\partial \theta_i}{\partial r}; \qquad i = 1, 2 \tag{25}$$

where the fluxes N_i are to be calculated using the Maxwell-Stefan equations. The set of coupled differential equations (25), along with the MS and RAST equations can be solved using the method of lines to obtain the transient loadings of *n*-C_6 and 3MP as a function of the dimensionless time; see Figure 15(a). The loading at any instant is calculated from the loading profiles within the spherical particle using:

$$\Theta_i = \frac{3}{r_c^3} \int_0^{r_c} \Theta_i \, r^2 dr \tag{26}$$

The *n*-C_6 loading increases with time as expected. The 3MP loading in the particle exhibits a curious maximum near the start of the uptake process and subsequently the loading decreases with increasing time. In order to understand the maximum loading of 3MP during transience, the transient profiles of the two isomers within the particle have been examined; see Figure 15(c) and (d). The *n*-C6 transience is as expected; the profiles relax to their equilibrium values in a monotonic manner. On the other hand the 3MP loading rises to a maximum within the particle

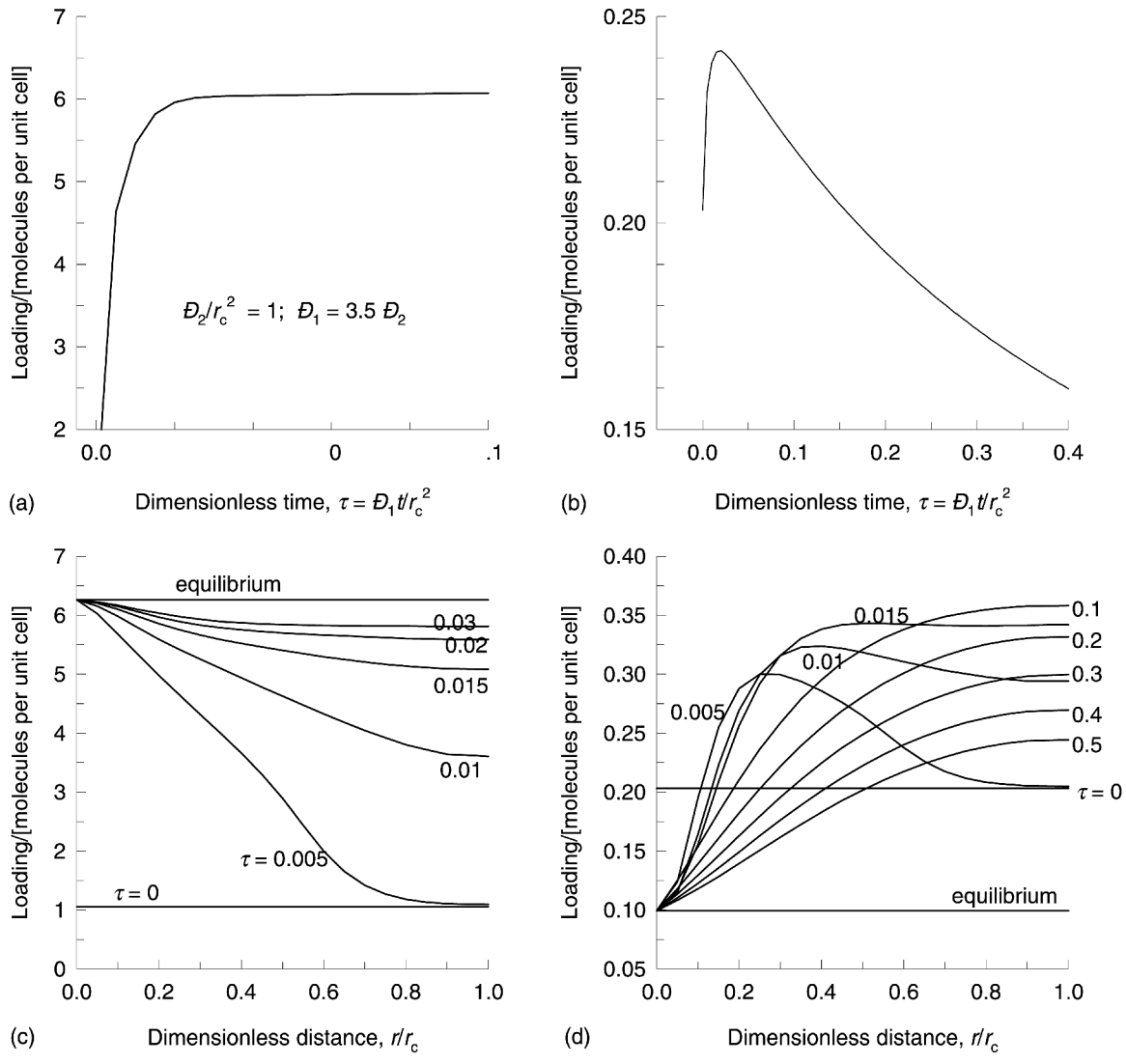

Figure 16. Transient uptake within silicalite particle of (a) *n*-C_6 and (b) 22DMB at 398 K. The particle is exposed to a 50-50 mixture at a total hydrocarbons pressure of 20 kPa. The loading profiles within the particle are shown in (c) and (d) for the isomers.

during the initial stages of the diffusion process. The maximum loading within the particle is higher than the final equilibrium value. As time progresses the maximum loading of 22DMB within the particle is dissipated and ''normal'' profiles are established. The curious behaviour of 3MP transient uptake, is to be entirely attributed to the maximum in the loading in the mixture; see Figure 7(b).

Exactly analogous results are obtained during transient uptake of *n*-C_6 and 22DMB from a 50-50 mixture at 398 K and total pressure of 20 kPa into a spherical crystal of silicalite; see Figure 16. The maximum in the 22DMB loading is even more pronounced than in the previous case.

In practice, one would use a packed bed adsorber filled with silicalite adsorbents and operate this column in a transient manner. Assuming plug flow of the vapour phase the vapour phase molar concentration of a component is given by (see Van den Broeke and Krishna[30] for details):

$$\frac{\partial c_i}{\partial t} = -\frac{\partial (u c_i)}{\partial z} - \left(\frac{1-\varepsilon}{\varepsilon}\right)\rho \frac{\partial \bar{q}_i}{\partial t} \tag{27}$$

where c_i is the molar concentration in the gas phase, u is the fluid phase velocity, z is the axial coordinate distance, ε is the bed porosity, ρ is the density of the silicalite adsorbent particles and $\bar{q}_i$ is the average concentration within the spherical particle:

$$\bar{q}_i = \frac{3}{r_c^3}\int_0^{r_c} q_i r^2 dr \tag{28}$$

The set of equations (26), (27) and (28) along with the Maxwell-Stefan and RAST equations can be solved using the numerical procedure described by Van den Broeke and Krishna[30]. The normalised breakthrough curves for a gaseous mixture with a total pressure of 100 kPa and partial pressures of *n*-C_6 and 3MP equal to 20 kPa each are shown in Figure 17(a). The residence time in the adsorber (L/u_0) was taken to be 80 s where u_0 is the superficial gas velocity at the inlet. The porosity of the packed bed $\varepsilon = 0.4$. The M-S diffusivities of the linear and branched alkanes are taken equal to each other, $Đ_1 = Đ_2$. The particle radius r_c was chosen such that $Đ_1/r_c^2 = 4 \times 10^{-7}\ s^{-1}$. The particle

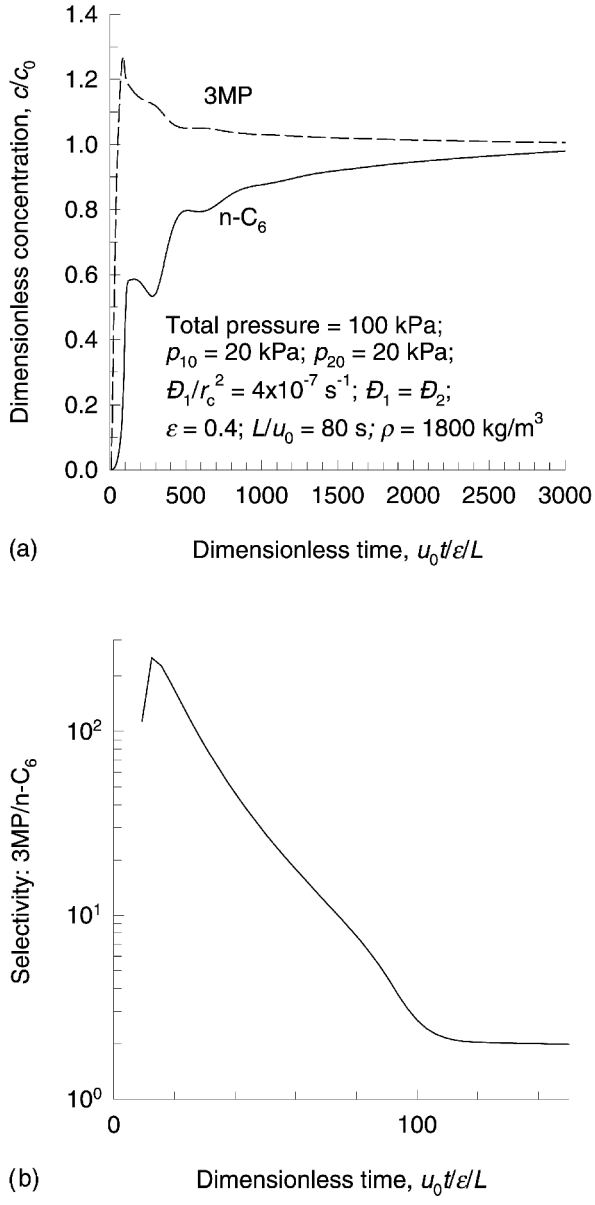

Figure 17. (a) Breakthrough curves in an adsorber packed with silicalite particles. The entering gas consists of a 50-50 mixture (a) *n*-C_6 and (b) 3MP at 362 K. (b) Breakthrough selectivity.

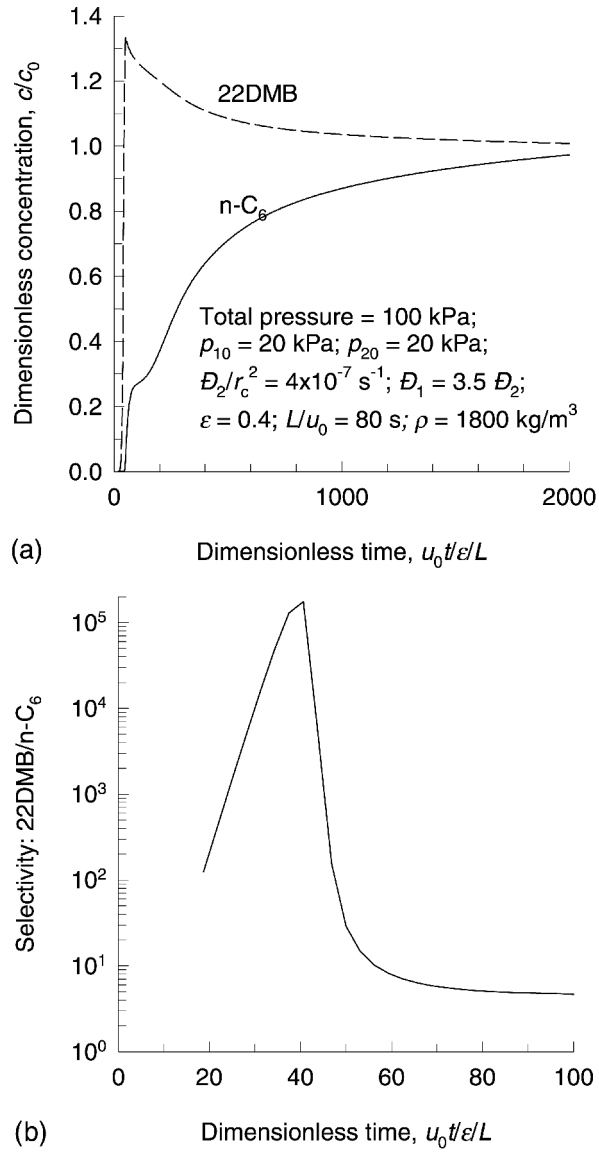

Figure 18. (a) Breakthrough curves in an adsorber packed with silicalite particles. The entering gas consists of a 50-50 mixture (a) *n*-C_6 and (b) 22DMB at 398 K. (b) Breakthrough selectivity.

density $\rho = 1800\ \text{kg m}^{-3}$. The exiting gas phase is rich in the branched isomer and the breakthrough selectivity is shown in Figure 17(b). The selectivity values during the initial stages is higher than for steady-state membrane permeation; compare Figure 13(c) with 17(b).

Analogous breakthrough curves were determined for a 50-50 mixture of *n*-C_6 and 22DMB; see Figure 18. The residence time in the adsorber (L/u_0) was taken to be 80 s where u_0 is the superficial gas velocity at the inlet. The porosity of the packed bed $\varepsilon = 0.4$. The M-S diffusivities of the linear and branched alkanes are taken such that, $Đ_1 = 3.5\,Đ_2$. The particle radius r_c was chosen such that $Đ_1/r_c^2 = 4 \times 10^{-7}\ \text{s}^{-1}$. The particle density $\rho = 1800\ \text{kg m}^{-3}$.

The high breakthrough selectivities observed for the two systems suggest that this process could have commercial potential.

7. CONCLUDING REMARKS

This paper demonstrates the power of CBMC simulations, in conjunction with the Maxwell-Stefan diffusion theory, for modelling separations of mixtures of hexane isomers. With the aid of CBMC simulations, it is shown that the extremely high selectivities reported by Funke *et al.*[14] and Gump *et al.*[15] for membrane separation of *n*-C_6 from 3MP and 22DMB, respectively, are primarily caused by the exclusion of the branched isomers from the zeolite. The reason for this exclusion is to be found in configurational entropy, or packing efficiency, effects.

The curious maximum in the 22DMB flux observed in the experiments of Gump *et al.*[15] is explained by the fact that in the experiments the hydrocarbons total pressure corresponded to conditions near the maximum in the loading of 22DMB in the mixture isotherms. Increase in the pressure for conditions to the left of the maximum leads to an increase in the 22DMB flux. On the other hand,

increase in the pressure to the right of the loading maximum leads to a decrease in the flux.

Breakthrough behaviour in a packed behaviour have been determined. These simulations show that high separation selectivities can be attained in this device.

NOTATION

A	surface area of adorbent, $m^2 kg^{-1}$
b_i	parameter in the Langmuir adsorption isotherm, Pa^{-1}
$[B]$	square matrix of inverse Maxwell-Stefan coefficients, $m^{-2} s$
D_{12}	Fick diffusivity of 1-2 binary in fluid mixture, $m^2 s^{-1}$
$[D]$	matrix of Fick diffusivities, m^2
$Đ_i$	Maxwell-Stefan diffusivity of species i in zeolite, m^2
$Đ_{ij}$	Maxwell-Stefan diffusivity describing interchange between i and j, m^2
N_i	molecular flux of species i, molecules $m^{-2} s^{-1}$
P	system pressure, Pa
P_i^0	vapour pressure analog in equation (4), Pa
p_i	partial pressure of species i, Pa
q_i	molar loading of component i, mol kg^{-1}
$q_{i,sat}$	saturation loading of component i, mol kg^{-1}
r_c	radius of spherical crystal, m
R	gas constant, 8.314 J mol^{-1} K^{-1}
t	time, s
T	absolute temperature, K
x_i	mole fraction of species i, dimensionless
z	distance coordinate along membrane, m
z	number of nearest neighbour sites in Figure 11, dimensionless

Greek letters

δ	thickness of membrane, m
ε	porosity of packed bed, dimensionless
γ_1	activity coefficient of species i, dimensionless
Γ	thermodynamic correction factor, dimensionless
$[\Gamma]$	matrix of thermodynamic factors, dimensionless
θ_i	fractional surface occupancy of component i
Θ_i	molecular loading, molecules per unit cell or per cage
$\Theta_{i,sat}$	saturation loading, molecules per unit cell or per cage
$\Theta_{i\,sat,A}$	maximum loading of site A, molecules per unit cell
$\Theta_{i\,sat,B}$	maximum loading of site B, molecules per unit cell
Λ_{ij}	Wilson parameters, dimensionless
λ	lateral displacement, m
μ_i	molar chemical potential, J mol^{-1}
ν	jump frequency, s^{-1}
π	spreading pressure, Pa m
ρ	density, number of unit cells per m^3 or kg m^{-3}
τ	dimensionless time, $\tau \equiv (tĐ_1/r_c^2)$

Subscripts

A	referring to site A
B	referring to site B
1	component 1 in binary mixture
2	component 2 in binary mixture
max	referring to maximum loading
sat	referring to saturation conditions
i, j	components in mixture
p	derivative at constant pressure
T,p	derivative at constant temperature and pressure

Superscripts

0	pure component parameter

Vector and matrix notation

( )	component vector
[ ]	square matrix

Operators

∇	gradient or nabla

REFERENCES

1. Kärger, J. and Ruthven, D. M., 1992, *Diffusion in Zeolites and Other Microporous Solids* (Wiley, New York).
2. Ruthven, D. M., Farooq, S. and Knaebel, K. S., 1994, *Pressure Swing Adsorption*, (VCH Publishers, New York).
3. Reid, R. C., Prausnitz, J. M. and Poling, B. M., 1988, *The Properties of Gases and Liquids*, Fourth Edition, (McGraw-Hill, New York).
4. Smit, B. and Maesen, T. L. M., 1995, *Commensurate* ''Freezing'' of Alkanes in the Channels of a Zeolite, *Nature*, 374: 42–44.
5. Sun, M. S., Talu, O. and Shah, D. B., 1996, Adsorption equilibria of C_5– C_{10} normal alkanes in silicalite crystals, *J Phys Chem*, 100: 17276–17280.
6. Sun, M. S., Shah, D. B., Xu, H. H. and Talu, O., 1998, Adsorption equilibria of C_1– C_4 alkanes, CO_2 and SF_6 on silicalite, *J Phys Chem*, 102: 1466–1473.
7. Vlugt, T. J. H., Martin, M. G., Siepmann, J. I., Smit, B. and Krishna, R., 1998, Improving the efficiency of the CBMC algorithm, *Molecular Physics*, 94: 727–733.
8. Krishna, R., Smit, B. and Vlugt, T. J. H., 1998, Sorption-induced diffusion-selective separation of hydrocarbon isomers using silicalite, *J Phys Chem A*, 102: 7727–7730.
9. Vlugt, T. J. H., Zhu, W., Kapteijn, F., Moulijn, J. A., Smit, B. and Krishna, R., 1998, Adsorption of linear and branched alkanes in the zeolite silicalite-1, *J Am Chem Soc*, 120: 5599–5600.
10. Krishna, R., Vlugt, T. J. H. and Smit, B., 1999, Influence of isotherm inflection on diffusion in silicalite, *Chem Eng Sci*, 54: 1751–1757.
11. Vlugt, T. J. H., Krishna, R. and Smit, B., 1999, Molecular simulations of adsorption isotherms of linear and branched alkanes and their mixtures in silicalite, *J Phys Chem B*, 103: 1102–1118.
12. Krishna, R. and Paschek, D., 2000, Permeation of hexane isomers across ZSM-5 zeolite membranes, *Ind Eng Chem Res*, 39: 2618–2622.
13. Krishna, R. and Paschek, D., 2000, Separation of Hydrocarbon Mixtures using Zeolite Membranes: A modelling approach combining molecular simulations with the Maxwell-Stefan theory, *Separation and Purification Technology*, 21: 111–136.
14. Funke, H. H., Argo, A. M., Falconer, J. L. and Noble, R. M., 1997, Separation of cyclic, branched, and linear hydrocarbon mixtures through silicalite membranes, *Ind Eng Chem Res*, 36: 137–143.
15. Gump, C. J., Noble, R. D. and Falconer, J. L., 1999, Separation of Hexane Isomers through Nonzeolite Pores in ZSM-5 Zeolite Membranes, *Ind Eng Chem Res*, 38: 2775–2781.
16. Frenkel, D. and Smit, B., 1996, Understanding molecular simulations: from algorithms to applications, (Academic Press, San Diego).
17. Calleja, G., Jimenez, A., Pau, J., Dominguez, L. and Perez, P., 1994, Multicomponent adsorption equilibrium of ethylene, propane, propylene and CO_2 on 13X zeolite, *Gas Separation and Purification*, 8: 247–256.
18. Krishna, R., 1990, Multicomponent surface diffusion of adsorbed species. A description based on the generalized Maxwell-Stefan diffusion equations, *Chem Eng Sci*, 45: 1779–1791.
19. Krishna, R., 1993, Problems and Pitfalls in the use of the Fick Formulation for Intraparticle Diffusion, *Chem Eng Sci*, 48: 845–861.
20. Krishna, R. and Wesselingh, J. A., 1997, The Maxwell-Stefan approach to mass transfer, *Chem Eng Sci*, 52: 861–911.
21. Kapteijn, F., Moulijn, J. A. and Krishna, R., 2000, The Generalized Maxwell-Stefan model for diffusion in zeolites: Sorbate molecules with different saturation loadings, *Chem Eng Sci*, 55: 2923–2930.
22. Keil, F. J., Krishna, R. and Coppens, M. O., 2000, Modeling of Diffusion in Zeolites, *Reviews in Chemical Engineering*, 16: 71–197.
23. Krishna, R., 2000, Diffusivity of binary mixtures in zeolites: MD simulations vs Maxwell-Stefan theory, *Chemical Physics Letters*, 326: 477–484.
24. Paschek, D. and Krishna, R., 2001, Diffusion of binary mixtures in zeolites: Kinetic Monte Carlo vs Molecular Dynamics simulations, *Langmuir*, 17: 247–254.
25. Paschek, D. and Krishna, R., 2001, Inter-relation between self- and jump-diffusivities in zeolites, *Chem Phys Lett*, 333: 278–284.
26. Vignes, A., 1966, Diffusion in binary solutions, *Ind Eng Chem Fundam*, 5: 189–199.
27. Habgood, H. W., 1958, The kinetics of molecular sieve action. Sorption of nitrogen-methane mixtures by Linde molecular sieve 4A, *Can J Chem*, 36: 1384–1397.
28. Round, G. J., Habgood, H. W. and Newton, R., 1966, A numerical analysis of surface diffusion in a binary adsorbed film, *Separation Science*, 1: 219–244.
29. Schiesser, W. E., 1991, *The numerical method of lines: Integration of partial differential equations*, (Academic Press, San Diego).

30. Van den Broeke, L. J. P. and Krishna, R., 1995, Experimental verification of the Maxwell-Stefan theory for micropore diffusion, *Chem Eng Sci*, 50: 2507–2522.

ACKNOWLEDGEMENTS

RK acknowledges a grant '*Programmasubsidie*' from the Netherlands Foundation for Fundamental Research (CW-NWO) for development of novel concepts in reactive separations. J. M. van Baten provided valuable programming assistance. D. Paschek assisted in providing the CBMC simulation results.

ADDRESS

Correspondence concerning this paper should be addressed to Professor R. Krishna, Department of Chemical Engineering, University of Amsterdam, Nieuwe Achtergracht 166, 1018WV Amsterdam, The Netherlands.

The manuscript was received 27 July 2000 and accepted for publication after revision 4 December 2000.